NASA TECHNICAL MEMORANDUM

NASA TM X-1780

NASA TM X-1780

STEADY-STATE INTERACTIONS FROM MACH 1.98 TO 2.58 BETWEEN A TURBOJET ENGINE AND AN AXISYMMETRIC INLET WITH 60-PERCENT INTERNAL AREA CONTRACTION

by Robert E. Coltrin and David A. Choby

Lewis Research Center
Cleveland, Ohio

NATIONAL AERONAUTICS AND SPACE ADMINISTRATION • WASHINGTON, D. C. • APRIL 1969

NASA TM X-1780

STEADY-STATE INTERACTIONS FROM MACH 1.98 TO 2.58 BETWEEN A TURBOJET ENGINE AND AN AXISYMMETRIC INLET WITH 60-PERCENT INTERNAL AREA CONTRACTION

By Robert E. Coltrin and David A. Choby

Lewis Research Center
Cleveland, Ohio

NATIONAL AERONAUTICS AND SPACE ADMINISTRATION

For sale by the Clearinghouse for Federal Scientific and Technical Information
Springfield, Virginia 22151 – CFSTI price $3.00

ABSTRACT

An investigation of the steady-state interactions between a Mach 2.5 axisymmetric mixed-compression inlet and a turbojet engine has been conducted. Engine installation did not grossly alter the magnitude or distribution of total pressure at the inlet diffuser exit from the values obtained with a choked plug installed. However, when a large circumferential total-pressure distortion was present at the compressor face, the engine altered the flow field by inducing a circumferential distortion in the static pressure without significantly affecting the total-pressure profile. Limited data at a constant speed showed that large radial distortions caused a slight loss in compressor pressure ratio.

STEADY-STATE INTERACTIONS FROM MACH 1.98 TO 2.58 BETWEEN A TURBOJET ENGINE AND AN AXISYMMETRIC INLET WITH 60-PERCENT INTERNAL AREA CONTRACTION

by Robert E. Coltrin and David A. Choby

Lewis Research Center

SUMMARY

An investigation of the steady-state interactions between a high-performance inlet and a J85-GE-13 turbojet engine has been conducted in the Lewis 10- by 10-Foot Supersonic Wind Tunnel over the 1.98 to 2.58 Mach range. The inlet was an axisymmetric mixed-compression type with a design Mach number of 2.5 and 60-percent internal area contraction.

Angle of attack was investigated at the nominal Mach numbers of 2.5 and 2.6. Engine installation did not grossly alter the magnitude or distribution of total pressure at the inlet diffuser exit from the magnitude and distribution obtained with a choked plug installed. However, when a large circumferential total-pressure distortion existed, the engine induced a circumferential static-pressure distortion at the compressor face. This distortion caused a more uniform distribution of corrected airflow at the compressor face. Also, a circumferential work gradient in the compressor was associated with the large circumferential total-pressure distortion at the compressor face. Limited data showed that large radial distortions caused a slight loss in compressor pressure ratio at constant corrected speed. This loss was noted especially at Mach 1.98 when a radial total-pressure distortion of 0.26 caused a 5 percent loss in compressor pressure ratio.

INTRODUCTION

The proper operation and control of a supersonic aircraft propulsion system requires a knowledge of the steady-state and dynamic interactions between the inlet and the engine. In order to investigate this area and the associated control problems, an experimental program is being conducted in the Lewis 10- by 10-Foot Supersonic Wind Tunnel. For the initial tests, an axisymmetric inlet was selected with a design Mach number of 2.5

and with 60 percent of the supersonic area contraction occurring internally. A complete discussion of the aerodynamic design of the inlet is presented in reference 1. Experimental investigations have optimized the porous bleed system, examined the effect of bleed system backpressure, studied the performance characteristics of the inlet system with bypasses operating, determined the response of the terminal shock to external and internal disturbances, and developed the inlet overboard bypass control system. The results of these investigations are presented in references 1 to 5, respectively.

Before an attempt can be made to study the dynamic interactions between the inlet and engine, the steady-state interactions must first be known. The present report presents an experimental study of the steady-state interactions between the inlet described in reference 1 and a J85-GE-13 turbojet engine. Previous steady-state studies (refs. 6 and 7) have shown that the presence of an engine does not significantly alter the inlet performance and that high inlet distortion does not appreciably affect the steady-state performance of the engine about its normal operating line. However, these studies were performed using engines which had low compressor stage loadings. Therefore, the present tests were performed to investigate steady-state inlet-engine compatibility with an engine of more advanced design which incorporates a compressor with a high pressure ratio per stage. The tests investigated the effect of engine installation on the flow at the compressor face station and the effect of inlet steady-state distortion on engine performance. The study included nominal Mach numbers of 2.0, 2.3, 2.5, and 2.6. Angle of attack was investigated at the nominal Mach numbers of 2.5 and 2.6. It is recognized that the dynamic fluctuations which are superimposed on the steady-state distortion may affect engine operation; however, for these tests, instrumentation was limited to steady-state measurements.

SYMBOLS

A	area, cm^2
H	total height of annulus at given station, cm
h	distance from centerbody surface, cm
M	Mach number
N	engine speed, rpm
N*	design engine speed, 16 500 rpm
P	total pressure, N/m^2
ΔP_2	$P_{2,max} - P_{2,min}$, N/m^2

p	static pressure, N/m^2
Re	Reynolds number
T	total temperature, K
W	engine airflow, kg/sec
W_f	engine main fuel flow, kg/sec
α	angle of attack, deg
β	power-level angle, deg
γ	ratio of specific heats
δ	local $P/101\ 325\ N/m^2$
θ	local $T/288.1\ K$

Subscripts:

max	maximum
min	minimum
n	nominal
s	sector
0	freestream
2	compressor face station
3	compressor exit station
5	turbine exit station
8	nozzle exit station

Supercript:

$\overline{\quad}$	average

APPARATUS AND PROCEDURE

A cross section of the Mach 2.5 mixed-compression inlet used in this investigation is presented in figure 1. A translating centerbody was used for starting the inlet and for off-design operation. With the inlet operating at the design Mach number, 40 percent of the supersonic flow area contraction was external and 60 percent was internal. External compression was accomplished with a 12.5° half-angle conical centerbody. Internal compression was obtained from the oblique shock generated by the 0°

cowl lip and the two reflected oblique shocks plus isentropic compression between these reflected shocks.

The inlet configuration is identical to configuration IIND' of reference 3. Vortex generators were installed on the centerbody in the subsonic diffuser to prevent separation of flow from the centerbody in the bypass region when large overboard bypass flows were discharged. Performance bleed, which consisted of porous regions on the centerbody and cowl, was located both in the supersonic diffuser and in the throat region of the inlet. The total bleed removed by this system was about 5.5 percent of the capture mass flow. About 3 percent of the capture mass flow was bled through the secondary bypass and was used for engine cooling. The overboard bypass was used to match the inlet and engine airflows.

The cold-pipe and engine configurations are shown in figure 2. The J85-GE-13 turbojet engine had an eight-stage axial-flow compressor with a sea-level static military average pressure ratio per stage of 1.275 which yields an overall pressure ratio of 7.0. The compressor was driven by a two-stage turbine. The compressor interstage bleed valves (bleed was located after the third, fourth, and fifth compressor stages) and the inlet guide vanes were linked together and scheduled by the main fuel control as a function of corrected speed. This control also regulated fuel flow as a function of engine face temperature, compressor exit pressure, engine speed, and power-lever angle to control acceleration and steady-state speed. The afterburner fuel control regulated afterburner fuel flow as a function of compressor exit pressure and power-level angle. It also scheduled exhaust nozzle area as a function of power-lever angle until a control loop sensing turbine exit temperature would override the normal control and regulate the exhaust nozzle area to hold the turbine exit temperature at the rated value. Turbine exit temperature was held at the rated value during military and afterburner operation.

The compressor face instrumentation consisted of six 10-tube total-pressure rakes and six static-pressure taps each on the cowl and centerbody (fig. 3). The 10-tube rakes consisted of six equal-area-weighted tubes with additional tubes added on each side of the extreme equal-area-weighted tubes in positions corresponding to an 18-tube area-weighted rake. The total-pressure recoveries and distortions used to define a model condition, and which are stated in the legend or sublegends of the data figures, were obtained by using all 10 tubes in each rake. The data presented in figures 8, 9, 11, and 13 to 16(b) were also obtained using all 10 tubes in each rake. The data presented in figures 10, 12, and 16(c) and (d) were obtained by using the six area-weighted tubes in each rake which are indicated in figure 3. These data were shown as an average per sector, where a sector is a pie-shaped area equal to 1/6 of the flow area at the compressor face and centered about a total-pressure rake. The average total pressure per sector $\overline{P}_{2,s}$ is the average of the six area-weighted total-pressure tubes on the rake in that sector. The average static pressure per sector $\overline{p}_{2,s}$ is the average of the cowl and

centerbody static pressures located in the given sector. To calculate a correct airflow per sector, each sector was divided into the six equal areas centered about each of the six area-weighted tubes. For each area, the corrected airflow was determined by using the total-pressure tube in that area and a linear interpolation of the static pressure between the centerbody and cowl. The total corrected airflow per sector is then the summation of the six values calculated in each sector. The results of these calculations are presented in figure 10 (p. 22) as a percentage of the total engine corrected airflow. These rakes were located 21.3 centimeters upstream of the first rotor stage of the compressor. Differences between the cold-pipe total-pressure contours presented in reference 1 and those presented herein are due to the contours of reference 1 having been derived from 10 rakes rather than 6. Four of the rakes were removed before the engine tests, and therefore only the 6 rakes of figure 3 could be compared for both cold-pipe and engine configurations. Compressor face temperature was measured by two thermocouples (not shown in the figure) located 43 centimeters upstream of the first rotor stage of the compressor. The compressor discharge pressure was measured by the 16 radially area-weighted tubes located on the four rakes shown in figure 4(a). These rakes were located 1.3 centimeters downstream of the compressor final stator vanes. The compressor discharge temperatures were measured by the four thermocouples located on the four rakes shown in figure 4(a). The turbine discharge pressure was an average of the 20 area-weighted tubes located on the four rakes shown in figure 4(b). The turbine discharge temperature was measured by the eight thermocouples shown in figure 4(b), which were installed by the engine manufacturer and wired in parallel to give an average reading. A similar set of adjacent thermocouples (not shown in the figure) was used for the turbine exhaust temperature signal to the afterburner fuel control for exhaust nozzle area control. The engine speed was measured by a magnetic pickup which sensed the tooth passage of a rotating gear which was attached to the customer power takeoff shaft from the engine gearbox. The main fuel flow was measured by a turbine-type flowmeter. The position of the inlet guide vanes was measured by a potentiometer which was connected to the mechanical linkage of the vane drive system. The exhaust nozzle area was calculated from a potentiometer measurement of the translation of the nozzle actuation ring.

The tunnel conditions for all cold-pipe and engine testing are presented in table I. To obtain the higher tunnel total temperature at each Mach number, the natural-gas-fired tunnel air heater was used. The free-stream conditions resulting from tunnel air heater operation are presented in reference 8. The set values of the heater-on temperatures (which will be referred to as hot temperatures) were determined from an assumed supersonic aircraft flight schedule by attempting to match the relative variation in engine face total temperature with Mach number at Mach numbers less than the design value of 2.5. The maximum allowable compressor face temperature for the J85-GE-13 is 390 K, which was selected as the hot temperature at the nominal Mach numbers of 2.5 and 2.6. The

heater-off temperatures (which will be referred to as ambient temperatures) are the ambient tunnel total temperatures at the given Mach numbers.

The inlet had a capture area of 0.1758 square meter and supplied the engine airflow requirement during military operation at a free-stream Mach number of 2.5 and with a compressor inlet temperature of 390 K. At this compressor inlet temperature, military operation refers to engine operation at 101 percent mechanical speed and rated turbine discharge temperature. This operation results in an engine corrected speed $N/N^* \sqrt{\theta}$ of 0.869 and an engine corrected airflow $W\sqrt{\theta}/\delta$ of 15.83 kilograms per second. When the terminal shock was located just downstream of the geometric throat, the inlet supplied this engine airflow with a total-pressure recovery $\overline{P}_2/P_0$ of 0.924, which is 1 percent supercritical. Supercritical is defined as the drop in total-pressure recovery from the critical value computed as a percentage of the critical value. Critical is defined as the operating point with the terminal shock at the inlet geometric throat. At the ambient compressor inlet temperatures, the engine was operated at reduced power-lever angles which provided the same corrected speed and matched inlet and engine airflows. Reducing the power-lever angle increased the exhaust nozzle area and reduced mechanical speed so that the engine was no longer operating at a military rating. The hot and ambient temperature operating points virtually coincided on a compressor map. Slight variations were caused by the change in the exhaust nozzle area between the two conditions. At each Mach number, the engine was operated at both hot and ambient temperature conditions. Because the engine had to be operating at military rating before the afterburner was lit, all afterburner points were run with the tunnel air heater operating.

Figure 5 shows a time history of the engine windmill speed during a tunnel start. At about minus 8 minutes, the tunnel compressors were started with the tunnel pumped down to about 16 percent of atmospheric pressure. After the test section was supersonic at a nominal Mach number of 2.5, the tunnel total pressure was slowly increased to the level required to provide the desired test conditions. The engine windmill corrected speed was within 1 percent of 0.71 for all steady-state ambient temperature conditions shown in table I. The engine was always started with the tunnel at ambient temperature, and then the heater was turned on if desired. The engine speed was manually increased as the tunnel air temperature increased.

During the engine start transient in the tunnel, the inlet overboard bypass doors were operated on closed-loop control with the feedback being a throat exit static pressure. This control system (ref. 5) could hold the terminal shock near a given position in the inlet during an engine start from windmill conditions. The engine accelerated immediately after lightoff and increased its airflow demand 30 percent in about 0.5 second. Thus, the recovery was held at a high value and the distortion kept to a low value by automatic control of the overboard bypass doors. However, if the engine airflow demand

was too high, the overboard bypass doors would fully close and the inlet would operate supercritically.

Figure 6 shows the normalized fuel-flow parameter against speed map of the main fuel control for typical operating conditions. This map is built into the main fuel control in a nonnormalized form. The droop line for each power-lever-angle setting indicates the variation in metered fuel as engine speed changes. The acceleration schedule is the line that is followed during large power-lever-angle movements and is an upper limit for the fuel-flow parameter. The minimum fuel-flow parameter line is a lower limit for that parameter. The sea-level operating line is the locus of the steady-state operating points for sea-level static conditions and is determined by engine inlet and exhaust conditions and the scheduled exhaust nozzle area. In the control, the nonnormalized fuel-flow parameter for a given operating point is multiplied by the compressor discharge static pressure to determine main burner fuel flow for that point. Figure 7 shows the exhaust nozzle position schedule as a function of power-lever angle. If, for example, the engine operating at sea-level static conditions was accelerated from the idle setting at point A (fig. 6) by stepping the power-lever angle to 40°, the locus of the operating points as the engine increases speed would be from A straight up to B, along the acceleration schedule to C and then down the droop line to the steady-state operating point D. For tunnel conditions, a large pressure ratio is applied across the engine, and the sea-level static operating line is not followed. The steady-state operating point for tunnel conditions must be determined by using the tunnel operating lines (fig. 6), where each line represents a constant exhaust nozzle position. These lines are plotted for typical tunnel operating conditions which choke the exhaust nozzle even at windmill conditions. The steady-state operating point is the intersection of the droop line with the area line corresponding to the particular power-lever angle (see fig. 7).

If the engine, windmilling at 71 percent speed in the tunnel, were started by advancing the power-lever angle from off to an idle setting, which sets the nozzle at 92 percent of the maximum area (fig. 7), the speed would increase to about point E on the minimum fuel-flow parameter line (fig. 6), or to about 92 percent. This speed would force the inlet to operate about 12 percent supercritically even with the bypass doors fully closed. In order to circumvent such high-speed starts with high inlet distortion, it was necessary to ramp the throttle from off to a power-lever angle of 40° in 1 second with the igniter on. This procedure limited the steady-state speed after lightoff to about 89 percent (point F, fig. 6) by closing the nozzle about 60 percent of the maximum area (fig. 7). At this speed, the shock could be held in position by the bypass control system. There was no overshoot in speed or turbine discharge temperature during the start transient. This procedure produced successful lightoffs at all ambient temperature conditions listed in table I. The closed-loop overboard bypass door control system was operating not only

during engine ignition but also when the engine was shut down and when afterburner operation was initiated or terminated.

RESULTS AND DISCUSSION

Effects of Engine on Inlet

Using total-pressure distortion $\Delta P_2/\overline{P}_2$ as a comparative parameter, engine and cold-pipe data were compared to determine if the presence of the engine had any effect on the inlet flow. This comparison is presented in figure 8 for the test conditions shown in table I. At each Mach number, the supercritical data were obtained by two methods. The first was to keep the bypass area constant and increase engine speed. In the cold-pipe configuration, the engine speed variation was simulated by varying the area at the choked plug. The second method was to keep engine speed or choked-plug area constant and to increase the area of the overboard bypass. Both hot and ambient temperature data are shown. Points denoting afterburner operation are presented as tailed symbols. The agreement between the cold-pipe and engine configurations compared over a wide range of inlet conditions show that the presence of the engine did not affect the magnitude of the total-pressure distortions. Some disagreement in distortion occurs between the hot and ambient temperature data. Generally, the difference can be attributed to the change in Mach number due to heater operation (ref. 8). In addition, the spike position used for the hot data was optimum for the ambient temperature condition and, hence, was not necessarily optimum for the Mach number resulting from hot temperature operation. Figure 8 also shows that at 0° angle of attack the radial compressor face total-pressure distortion usually increased gradually as total-pressure recovery was decreased. However, figure 8(*l*) shows at a nominal Mach number of 2.0, 0° angle of attack, and ambient temperature, the total-pressure distortion remained constant at 0.09 until the recovery was decreased to 0.860 and then increased precipitously to 0.26 at 0.843 recovery. A similar phenomenon was observed for hot tunnel conditions. The distortion was radial; the large increase was due to nearly separated flow from the centerbody, which occurred only at a nominal Mach number of 2.0. It should be noted that the engine did not cause the near separation to occur since the same flow pattern was evident during cold-pipe operation.

To determine the effect of engine installation on the inlet flow, it is necessary to compare more than the magnitudes of total-pressure distortions. Figure 9 presents compressor face total-pressure contours at a nominal Mach number of 2.6, a nominal angle of attack of 4.5°, and ambient temperature for the engine and cold-pipe configurations. This condition provided the largest circumferential distortion encountered during

the test. These contours were plotted from data obtained from the six rakes shown in figure 3. It is shown in references 1 and 2 that data obtained from 10 rakes indicate three low-pressure lobes on the centerbody. These lobes were located angularly at the center of each of the three ducts. However, these lobes could not be observed with the existing engine instrumentation and were, therefore, ignored in this comparison. The engine was operated at 0.86 corrected speed $N/N^*\sqrt{\theta}$, and the cold-pipe plug was set to demand the same airflow.

Figure 9(a) represents a case where the engine was matched to the inlet, while parts (b) and (c) were supercritical cases obtained by opening the overboard bypass doors. Figures 9(d) to (f) show a similar series of cold-pipe points. There was no significant difference in cold-pipe and engine contours that could be attributed to the presence of an engine. The differences that do exist are attributed to the slight differences in pressure recoveries and angles of attack between the cold-pipe and engine data. The trends with pressure recovery for the cold-pipe and engine data are similar. For all cases, there is a deficiency of high-energy air in the lower ducts, which is as expected at positive angle of attack. Also, the high-energy air in the top duct tends to relocate near the centerbody as the total-pressure recovery is lowered for both the cold-pipe and engine data. The effect of the engine installation on compressor face pressures is shown in the distribution of static pressure. The cold pipe had at most a 2 percent difference in static pressure between the top and bottom ducts, while the engine configuration had as much as 6 percent difference.

Figure 10 shows the effect of the engine on the flow upstream of the compressor for the conditions of figures 9(b) and (e). The data in figure 10 are presented as an average per sector, where a sector is a pie-shaped area equal to 1/6 of the flow area and centered about a total-pressure rake as described in APPARATUS AND PROCEDURE. The total-pressure distribution was the same with or without the engine installed. For the cold-pipe configuration, static pressures around the inlet were nearly equal, but engine installation caused considerable difference in static pressure around the inlet. To determine the net effect of engine installation, a per-sector corrected airflow was calculated. The results of these calculations are presented as a percentage of the total engine corrected airflow.

The net result of installing the engine was a redistribution of the corrected airflow. The engine installation altered the static-pressure distribution at the compressor face and did not affect the total-pressure profile. Therefore, it is evident (assuming a uniform total temperature at the engine face) that the redistribution of corrected airflow $W\sqrt{\theta}/\delta$ was due to a redistribution of actual airflow W and not to a change in the total-temperature ratio θ or in the total-pressure ratio δ. The corrected airflow variation around the inlet at the compressor face was decreased from 8 percent to 4 percent of the total corrected airflow by the presence of the engine. These data (fig. 10) were meas-

ured at station 2, which is located 21.3 centimeters upstream of the first rotor stage of the compressor. The main duct is divided into three separate ducts 49 centimeters upstream of station 2. Thus, the major readjustment of corrected airflow indicated at station 2 is a readjustment of flow from one duct to another. Consequently, it must take place upstream of the struts. Between station 2 and the compressor face, any further flow readjustment that occurs must take place within each duct.

Effects of Inlet on Engine

The effect of inlet flow distortion on the compressor discharge pressure distributions is shown in figure 11. Figure 11(a) shows the compressor face total-pressure profiles and the corresponding compressor discharge total-pressure profiles for a case of low compressor face distortion at Mach 2.5, 0° angle of attack, and ambient temperature. Figure 11(b) shows similar profiles for the large radial and circumferential compressor face distortions obtained at Mach 2.58, 4.3° angle of attack, and ambient temperature. In both cases, the total-pressure distortion at the compressor exit was 0.05. The compressor exit total-pressure distortion varied between 0.04 and 0.05 for all data obtained and was independent of compressor face conditions. Thus, the effect of the compressor was to smooth out large circumferential and radial total-pressure distortions. At 4.3° angle of attack, where the compressor face was subjected to a large circumferential total-pressure distortion, the only means of obtaining uniform circumferential total pressure at the compressor exit was for the compressor to operate with a circumferential work gradient. Figure 12(a) shows the compressor face total-pressure recovery per sector, and figure 12(b) shows the compressor exit total temperatures, both as a function of circumferential position for Mach 2.58, 0° and 4.3° angles of attack, and ambient temperature. At 0° angle of attack, there was very little compressor face circumferential total-pressure distortion and very little compressor exit circumferential temperature variation. However, at 4.3° angle of attack, there was a large circumferential compressor face total-pressure distortion and a corresponding circumferential compressor exit temperature variation. Figure 12 indicates that the portion of the compressor that has the highest temperature rise does the most compression and therefore performs the most work.

Figure 13 shows compressor pressure ratio as a function of engine corrected speed for all Mach numbers tested at ambient temperatures and 0° angle of attack with the engine operating so that the nozzle was on the cruise flat (i.e., the nozzle exit area was constant at about 56 percent of the maximum area). Solid symbols indicate a compressor face radial total-pressure distortion of 0.20 or greater. The total-pressure distortion at Mach numbers of 2.50 and 2.30 did not reach values of 0.20, and there was no loss in compressor performance. There was a slight loss in compressor pressure ratio at

Mach 2.58 for the case of high distortion. At Mach 2.02 the effect of high distortion on compressor pressure ratio is more noticeable. The loss of compressor pressure ratio at a constant corrected speed of 0.938 was from 5.54 to 5.27, or a loss of almost 5 percent. Figure 14 shows typical rake profiles for the high and low distortion points at Mach 2.02. This figure shows, as previously discussed in Effects of Engine on Inlet, that the large radial distortion at the nominal Mach number of 2.0 was due to nearly separated flow from the centerbody. Thus, the compressor may be sensitive to hub radial distortion patterns.

Figure 15 shows various engine parameters as a function of engine corrected speed at Mach 2.58, 0° and 4.3° angles of attack, and ambient temperature. There is essentially no effect of angle of attack for corrected speeds below about 0.888. Above this point it takes more fuel at 4.3° angle of attack than at 0° to hold a given speed. The increase in fuel flow is reflected as an increase in other critical engine parameters, such as compressor pressure ratio (fig. 15(b)), engine total-temperature ratio (fig. 15(c)), and engine total-pressure ratio (fig. 15(d)). As shown in figure 15(e), the compressor interstage bleed valves followed the same schedule for 0° and 4.3° angles of attack. It appears from figure 15(f) that the nozzle schedule was the same for 0° and 4.3° angles of attack. Both of the data points at the highest corrected speeds were for cases where the exhaust nozzle area was scheduled to be on the steep slope between the cruise flat and military operation (see fig. 7). The power-lever angle for the 4.3°-angle-of-attack point was further advanced than it was for the 0°-angle-of-attack point. Therefore, the nozzle should have been further closed at 4.3° than at 0° angle of attack. The nozzle was scheduled to a further closed position at 4.3° angle of attack by the afterburner fuel control but the turbine exhaust temperature reached the rated value and the fuel control reopened the nozzle to hold the temperature at the rated value. Thus, the action of the fuel controls may have amplified the effect that the circumferential distortion had on the compressor at 4.3° angle of attack.

Figure 16 shows the compressor face total-pressure profiles and the circumferential compressor pressure ratios at Mach 2.58 for a high- and low-speed point and each at 0° and 4.3° angle of attack and ambient temperature. Only half of the compressor face is shown because of the symmetrical nature of the flow shown in figure 9. Figure 16(a) shows the compressor face total-pressure profiles for a relatively low speed where engine parameters were similar, and (b) shows comparable profiles for a higher speed where there was a difference in engine performance. In each case, there was a deficiency of high-energy air in the bottom two ducts (rake 3) for 4.3° angle of attack. Figures 16(c) and (d) show the circumferential variation of compressor pressure ratio for the same cases as figures 16(a) and (b), respectively. For 0° angle of attack, there is little circumferential variation in compressor pressure ratio. At 4.3° angle of attack, there is a large circumferential variation in compressor pressure ratio. This makes it

difficult to define exactly where the compressor is operating on its map. As pointed out before (fig. 11), the compressor exhausts the air at a nearly constant circumferential total pressure. Therefore, the bottom of the compressor must operate at a pressure ratio nearer to the stall line than the top since the bottom receives most of the low-pressure air. Thus, the compressor stall margin was locally reduced by a significant amount. As pointed out previously (fig. 15), the compressor pressure ratio at an engine speed of 0.86 was about the same at 4.3° and 0° angle of attack. This can also be seen from figure 16(c). However, figure 16(d) shows (as was shown in fig. 15) that at an engine corrected speed of 0.90, the average circumferential pressure ratio was greater at 4.3° than at 0° angle of attack. Also, the bottom portion of the compressor was operating near the zero distortion stall line at this condition.

SUMMARY OF RESULTS

An investigation of the steady-state interactions between a Mach 2.5 axisymmetric mixed-compression inlet and a J85-GE-13 turbojet engine has been conducted in the Lewis 10- by 10-Foot Supersonic Wind Tunnel. The test was conducted over the Mach range of 1.98 to 2.58 with the following results:

1. The engine did not grossly affect the magnitude or distribution of the total-pressure distortion at the compressor face.

2. At Mach 2.58 and 4.3° angle of attack with large circumferential compressor face total-pressure distortion, it was noted that (a) a circumferential distortion in the static pressure was induced by the engine at the compressor face, (b) a circumferential variation of corrected airflow was reduced from 8 percent to 4 percent of the total corrected airflow by engine installation, (c) there was a circumferential total-temperature distortion at the compressor exit, and (d) the stall margin of the compressor was locally reduced a significant amount.

3. The compressor exit total-pressure distortion remained constant at 0.04 to 0.05 for all inlet conditions, indicating the compressor had the ability to smooth out large radial and circumferential total-pressure distortions.

4. Limited data at a constant speed showed that large radial distortions tended to cause a loss in compressor pressure ratio.

Lewis Research Center,
National Aeronautics and Space Administration,
Cleveland, Ohio, January 20, 1969,
126-15-02-11-22.

REFERENCES

1. Cubbison, Robert W.; Meleason, Edward T.; and Johnson, David F.: Effect of Porous Bleed in a High-Performance Axisymmetric, Mixed-Compression Inlet at Mach 2.50. NASA TM X-1692, 1968.

2. Sanders, Bobby W.; and Cubbison, Robert W.: Effect of Bleed-System Back Pressure and Porous Area on the Performance of an Axisymmetric Mixed-Compression Inlet at Mach 2.50. NASA TM X-1710, 1968.

3. Cubbison, Robert W.; Meleason, Edward T.; and Johnson, David F.: Performance Characteristics from Mach 2.58 to 1.98 of an Axisymmetric Mixed-Compression Inlet System with 60-Percent Internal Contraction. NASA TM X-1739, 1969.

4. Wasserbauer, Joseph F.; and Willoh, Ross G.: Experimental and Analytical Investigation of the Dynamic Response of a Supersonic Mixed-Compression Inlet. Paper 68-651, AIAA, June 1968.

5. Crosby, Michael J.; Neiner, George H.; and Cole, Gary L.: High Performance Bypass Control for Mixed-Compression Inlets. Paper 68-652, AIAA, June 1968.

6. Bowditch, David N.; Anderson, Bernhard H.; and Tabata, William K.: Performance of a Turbojet Engine in Combination With an External-Internal-Compression Inlet to Mach 2.88. NASA TM X-254, 1960.

7. Beke, Andrew; Englert, Gerald; and Beheim, Milton A.: Effect of an Adjustable Supersonic Inlet on the Performance up to Mach Number 2.0 of a J34 Turbojet Engine. NACA RM E55I27, 1956.

8. Cubbison, Robert W.; and Meleason, Edward T.: Water Condensation Effects of Heated Vitiated Air on Flow in a Large Supersonic Wind Tunnel. NASA TM X-1636, 1968.

TABLE I. - TUNNEL CONDITIONS DURING TESTING OF COLD-PIPE AND ENGINE CONFIGURATIONS

Configuration	Nominal tunnel conditions			Actual tunnel conditions					
	Mach number, M_n	Total temperature, T_n	Angle of attack, α_n, deg	Free-stream Mach number, M_0	Free-stream total temperature, T_0, K	Free-stream total pressure, P_0, N/m^2	Ratio of specific heats, γ_0	Reynolds number per meter, Re/m	Angle of attack, α, deg
Engine	2.5	Hot	0 and 2.5	2.46	390	0.972×10^5	1.394	6.58×10^6	0 and 2.3
Cold pipe	↓	Hot	↓	2.47	390	.976	1.394	6.58	0 and 2.5
Engine	↓	Ambient	↓	2.50	294	.930	1.400	9.32	0 and 2.8
Cold pipe	↓	Ambient	↓	2.50	317	.896	1.400	8.10	0 and 2.8
Engine	2.6	Hot	0 and 4.5	2.54	390	1.078	1.394	6.99	0 and 4.3
Cold pipe	↓	Hot	↓	2.54	390	1.073	1.394	6.86	0 and 4.8
Engine	↓	Ambient	↓	2.58	339	1.051	1.400	8.30	0 and 4.3
Cold pipe	↓	Ambient	↓	2.58	372	1.045	1.400	7.50	0 and 4.8
Engine	2.3	Hot	0	2.34	361	.886	1.397	7.18	0
Cold pipe	↓	Hot	↓	2.34	361	.886	1.397	7.15	↓
Engine	↓	Ambient	↓	2.30	294	.858	1.400	9.54	↓
Cold pipe	↓	Ambient	↓	2.30	317	.810	↓	8.10	↓
Engine	2.0	Hot	↓	1.98	322	.652	↓	7.48	↓
Cold pipe	↓	Hot	↓	1.98	322	.652	↓	7.31	↓
Engine	↓	Ambient	↓	2.02	294	.661	↓	8.16	↓
Cold pipe	↓	Ambient	↓	2.02	317	.700	↓	7.97	↓

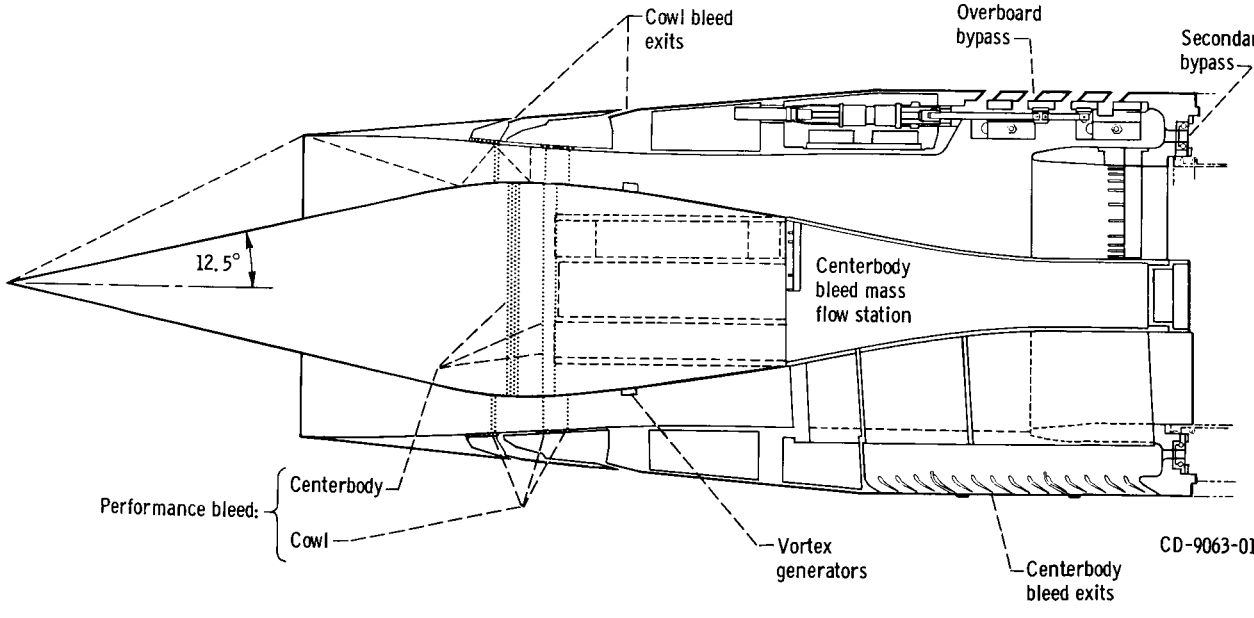

Figure 1. - Cross section of axisymmetric Mach 2.5 mixed-compression inlet.

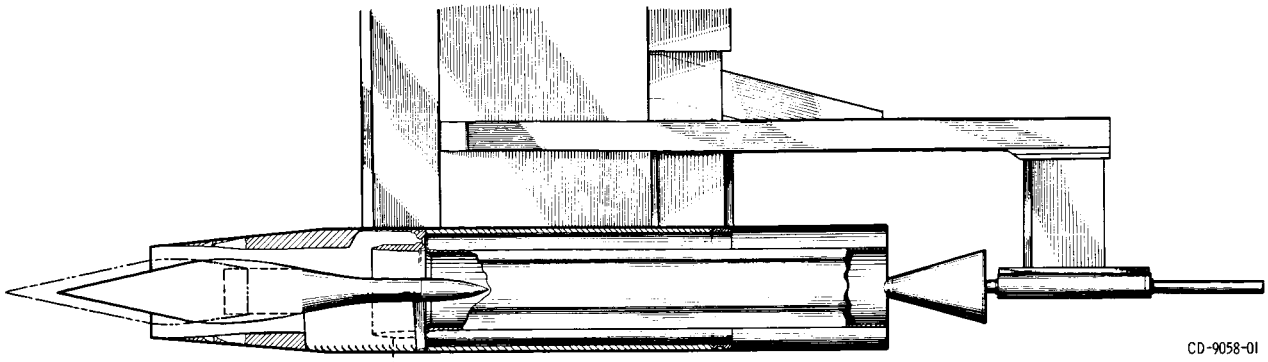

(a) Cold-pipe configuration.

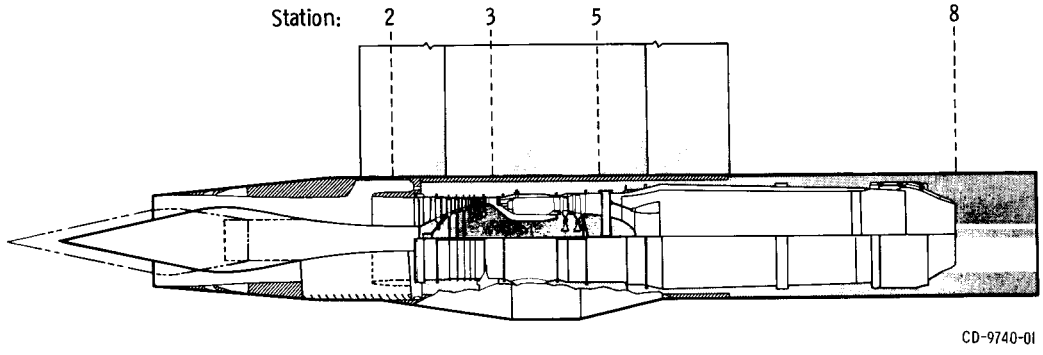

(b) Engine configuration.

Figure 2. - Cutaway of nacelle showing installation of cold-pipe and J85-GE-13 turbojet engine.

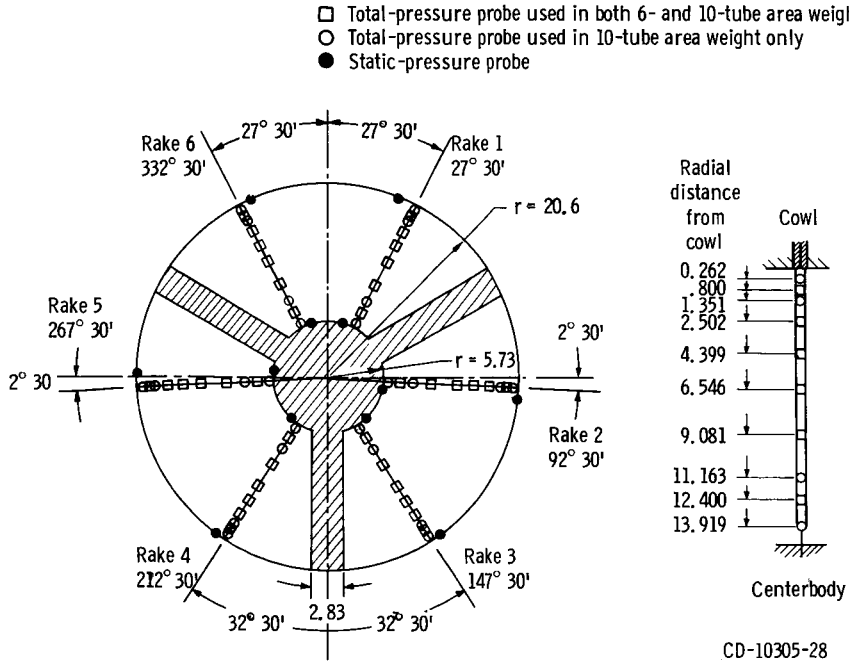

Figure 3. - Compressor face (station 2) instrumentation, looking downstream. Dimensions are in centimeters.

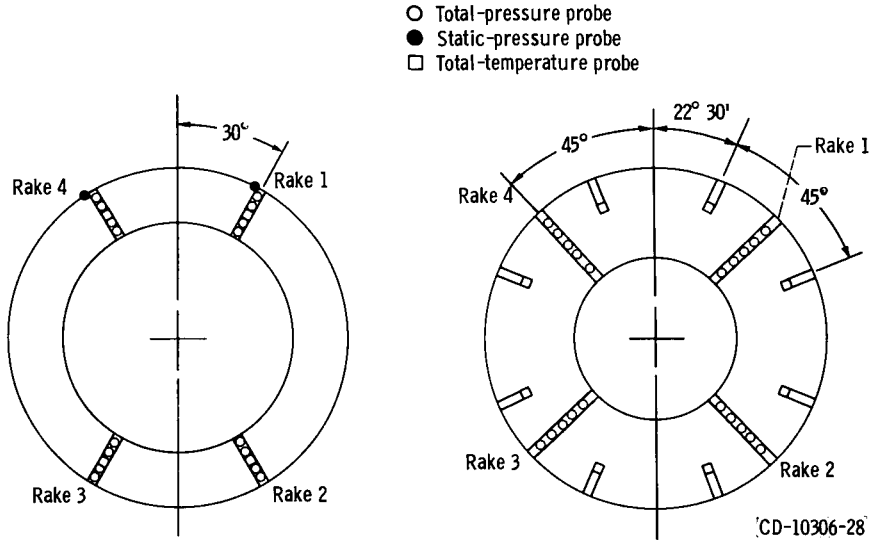

(a) Station 3 - compressor discharge.

(b) Station 5 - turbine discharge.

Figure 4. - J85-GE-13 engine instrumentation, looking downstream.

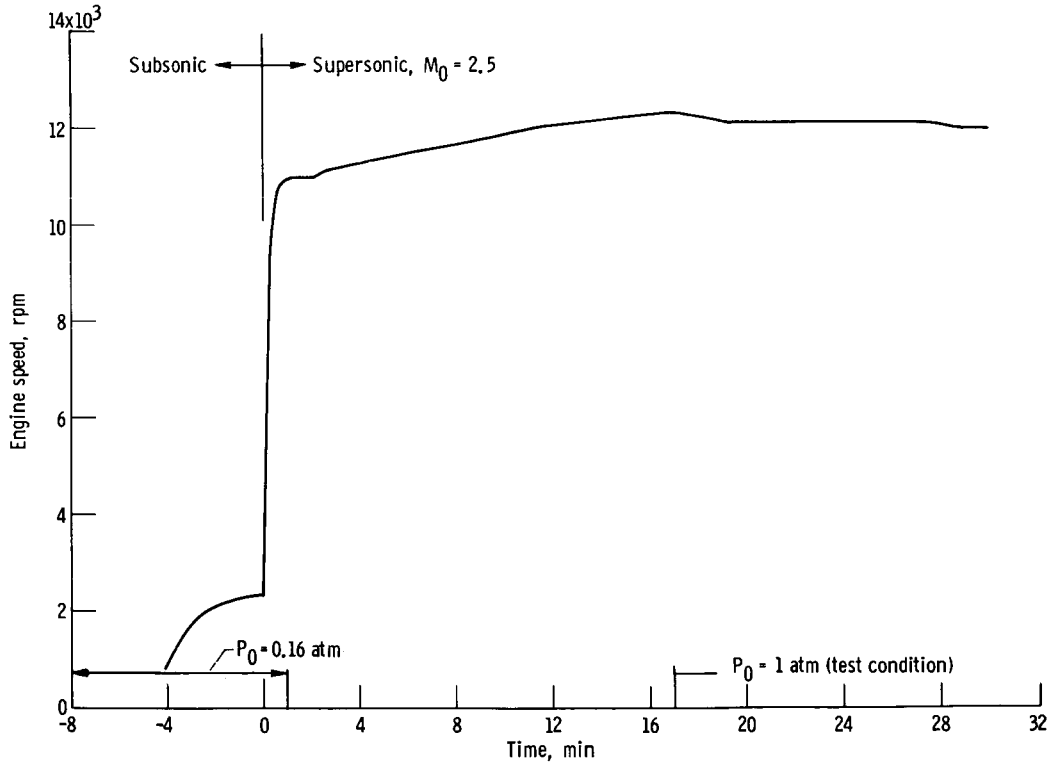

Figure 5. - Windmill speed of J85-GE-13 engine during tunnel start.

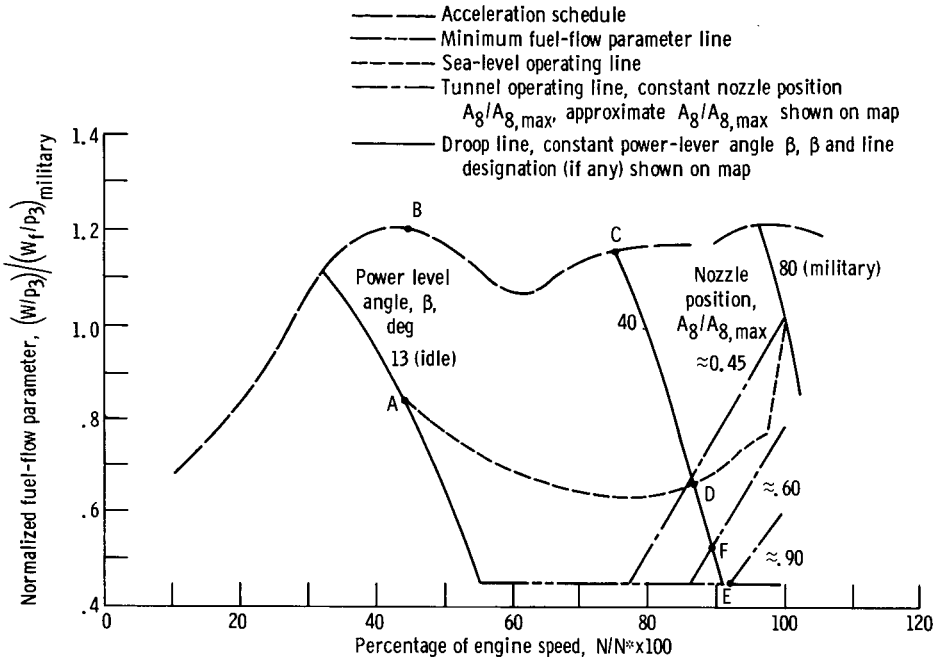

Figure 6. - Typical J85-GE-15 main fuel control operating schedule.

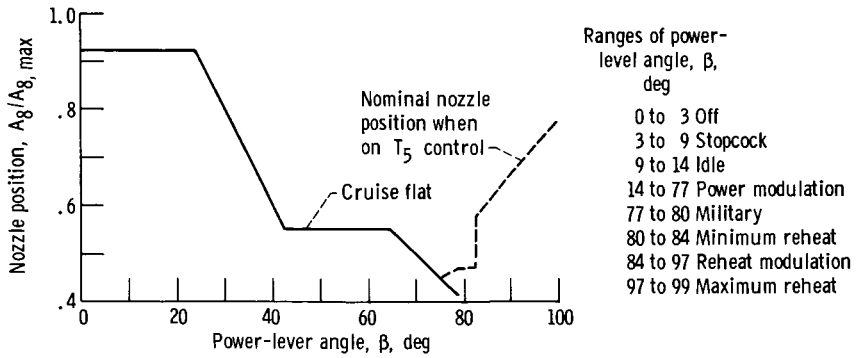

Figure 7. - J85-GE-13 nozzle position schedule. Maximum nozzle exit area, 1368 square centimeters.

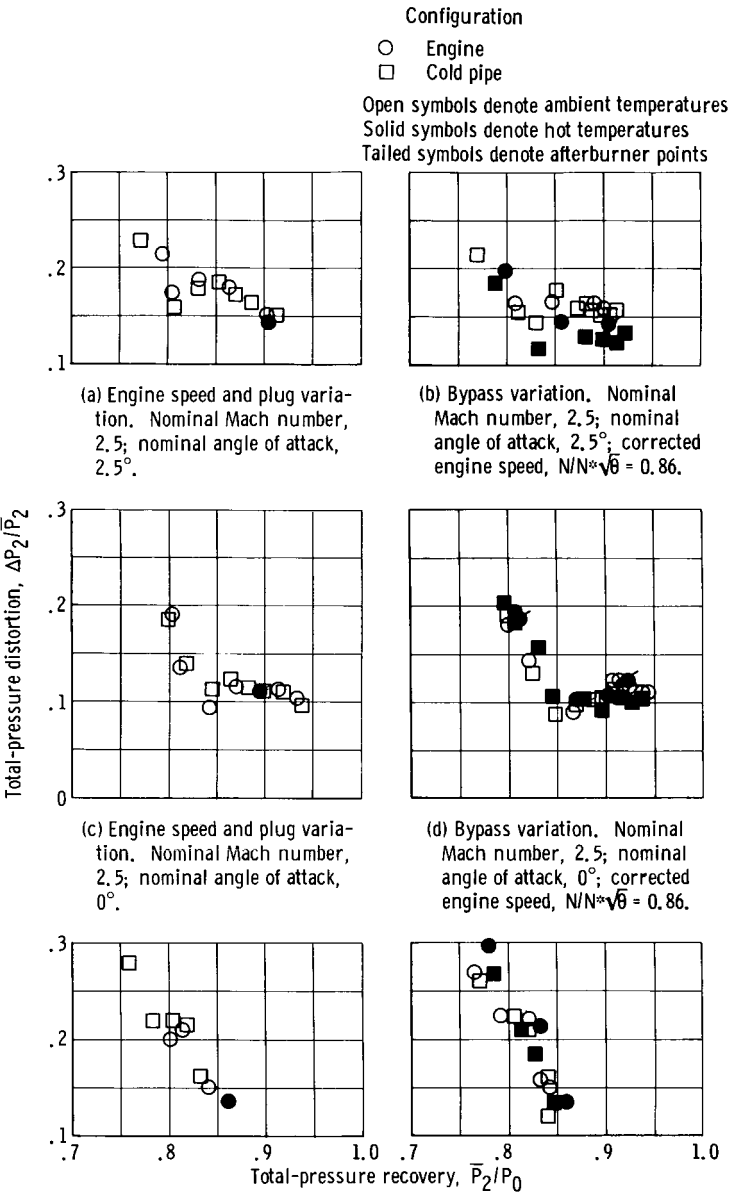

(a) Engine speed and plug variation. Nominal Mach number, 2.5; nominal angle of attack, 2.5°.

(b) Bypass variation. Nominal Mach number, 2.5; nominal angle of attack, 2.5°; corrected engine speed, $N/N^*\sqrt{\theta} = 0.86$.

(c) Engine speed and plug variation. Nominal Mach number, 2.5; nominal angle of attack, 0°.

(d) Bypass variation. Nominal Mach number, 2.5; nominal angle of attack, 0°; corrected engine speed, $N/N^*\sqrt{\theta} = 0.86$.

(e) Engine speed and plug variation. Nominal Mach number, 2.6; nominal angle of attack, 4.5°.

(f) Bypass variation. Nominal Mach number, 2.6; nominal angle of attack, 4.5°; corrected engine speed, $N/N^*\sqrt{\theta} = 0.86$.

Figure 8. - Effect of engine installation on total-pressure distortion at compressor face.

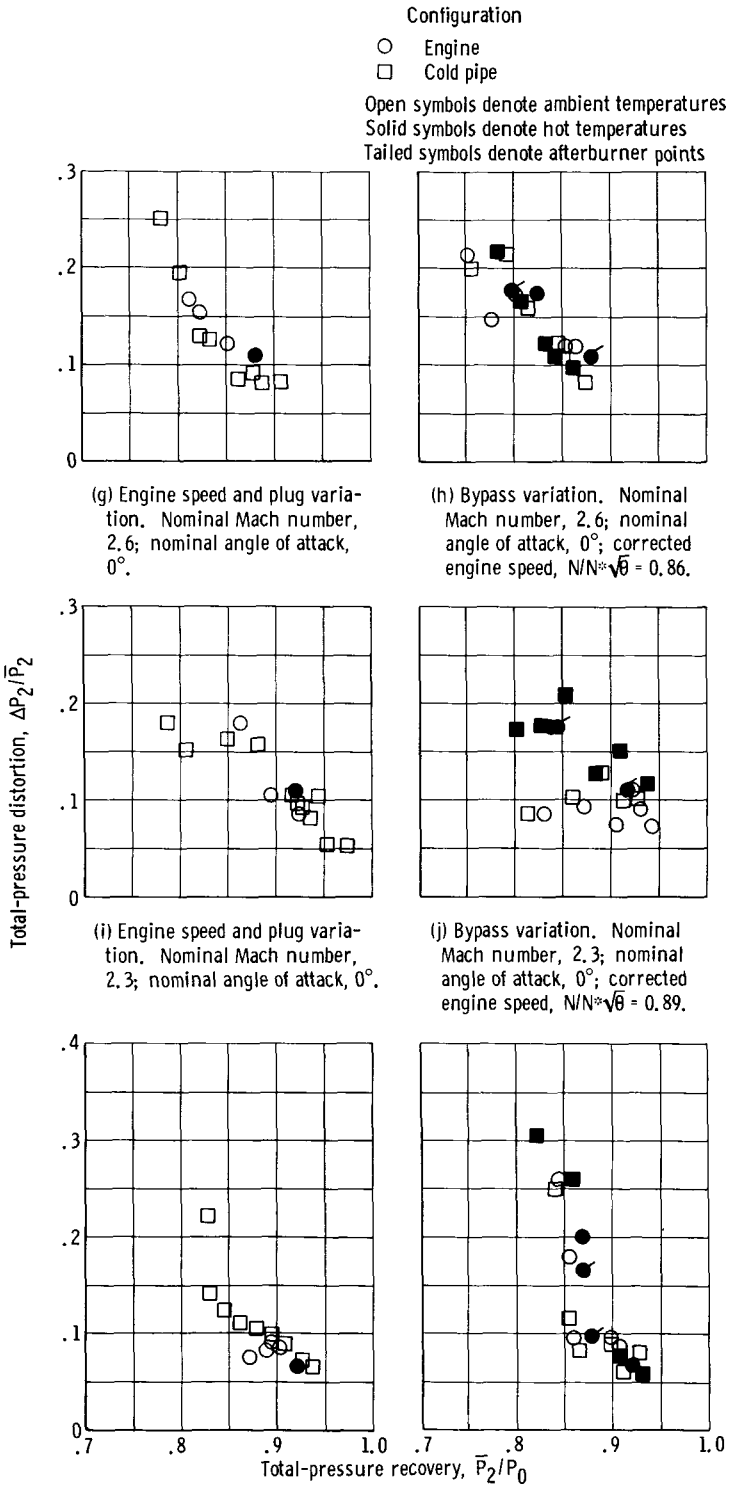

(g) Engine speed and plug variation. Nominal Mach number, 2.6; nominal angle of attack, 0°.

(h) Bypass variation. Nominal Mach number, 2.6; nominal angle of attack, 0°; corrected engine speed, $N/N^*\sqrt{\theta} = 0.86$.

(i) Engine speed and plug variation. Nominal Mach number, 2.3; nominal angle of attack, 0°.

(j) Bypass variation. Nominal Mach number, 2.3; nominal angle of attack, 0°; corrected engine speed, $N/N^*\sqrt{\theta} = 0.89$.

(k) Engine speed and plug variation. Nominal Mach number, 2.0; nominal angle of attack, 0°.

(l) Bypass variation. Nominal Mach number, 2.0; nominal angle of attack, 0°; corrected engine speed, $N/N^*\sqrt{\theta} = 0.94$.

Figure 8. - Concluded.

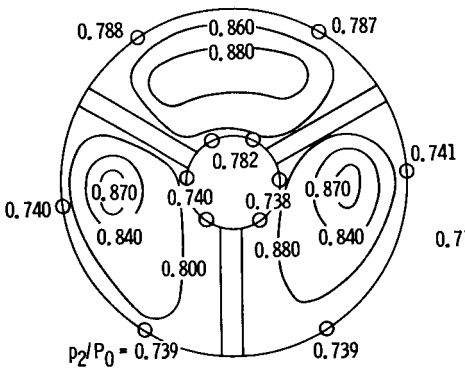

(a) Engine configuration. Total-pressure recovery, $\bar{P}_2/P_0 = 0.842$; total-pressure distortion, $\Delta P_2/\bar{P}_2 = 0.15$; corrected engine speed, $N/N^*\sqrt{\theta} = 0.86$.

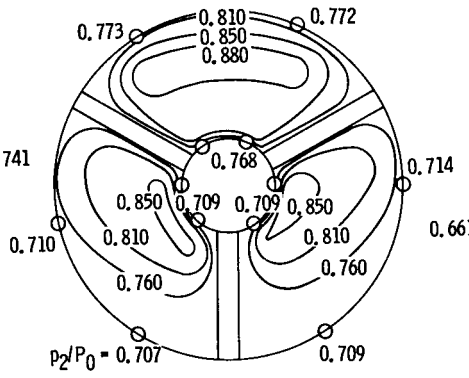

(b) Engine configuration. Total-pressure recovery, $\bar{P}_2/P_0 = 0.821$; total-pressure distortion, $\Delta P_2/\bar{P}_2 = 0.22$; corrected engine speed, $N/N^*\sqrt{\theta} = 0.86$.

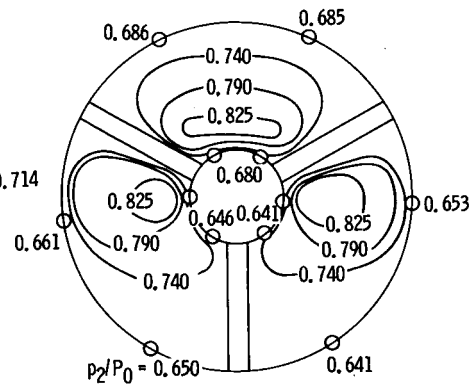

(c) Engine configuration. Total-pressure recovery, $\bar{P}_2/P_0 = 0.764$; total-pressure distortion, $\Delta P_2/\bar{P}_2 = 0.27$; corrected engine speed, $N/N^*\sqrt{\theta} = 0.86$.

CD-10307-28

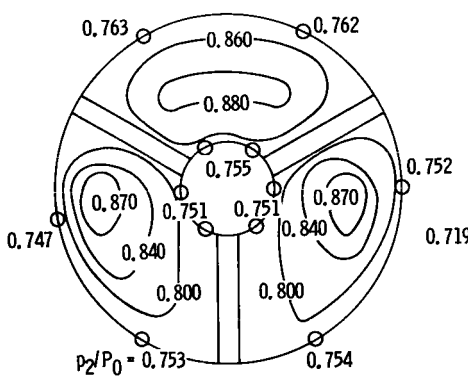

(d) Cold-pipe configuration. Total-pressure recovery, $\bar{P}_2/P_0 = 0.841$; total-pressure distortion, $\Delta P_2/\bar{P}_2 = 0.12$.

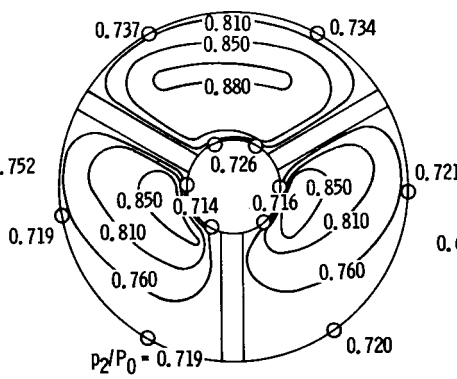

(e) Cold-pipe configuration. Total-pressure recovery, $\bar{P}_2/P_0 = 0.818$; total-pressure distortion, $\Delta P_2/\bar{P}_2 = 0.22$.

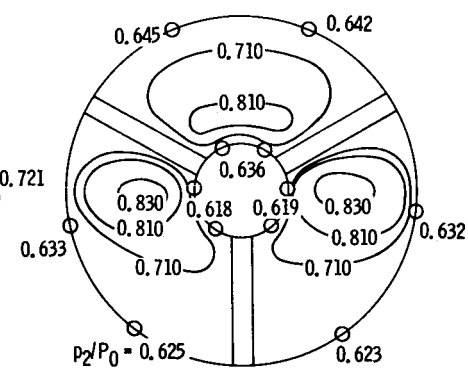

(f) Cold-pipe configuration. Total-pressure recovery, $\bar{P}_2/P_0 = 0.746$; total-pressure distortion, $\Delta P_2/\bar{P}_2 = 0.30$.

Figure 9. - Effect of engine installation on compressor face total-pressure-recovery contours at a nominal Mach number of 2.6, nominal angle of attack of 4.5°, and ambient temperature.

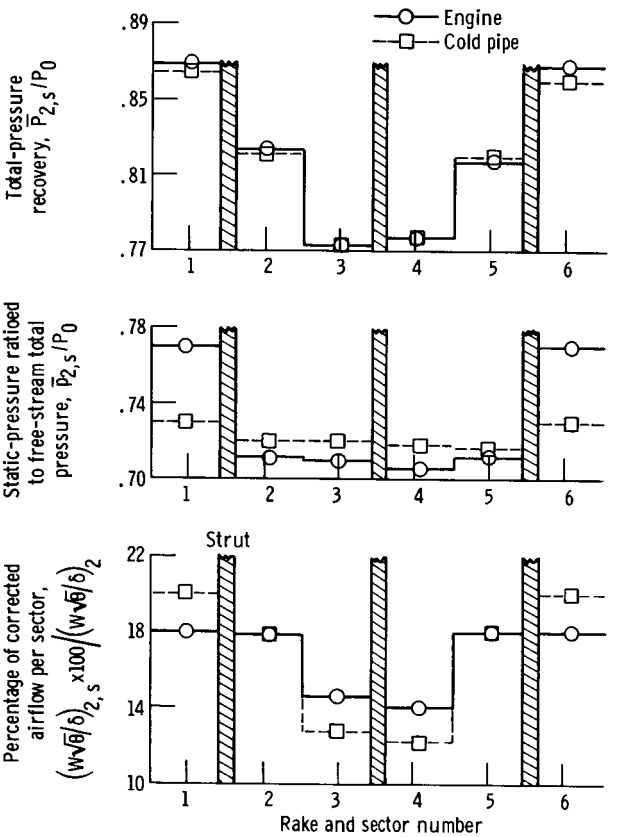

Figure 10. - Effect of engine on inlet. Nominal Mach number, 2.60; nominal angle of attack, 4.5°; corrected engine speed, $N/N^*\sqrt{\theta} = 0.86$; total-pressure recovery, $\bar{P}_2/P_0$: engine, 0.821; cold pipe, 0.818; total-pressure distortion, $\Delta P_2/\bar{P}_2$: engine and cold pipe, 0.22; ambient temperature.

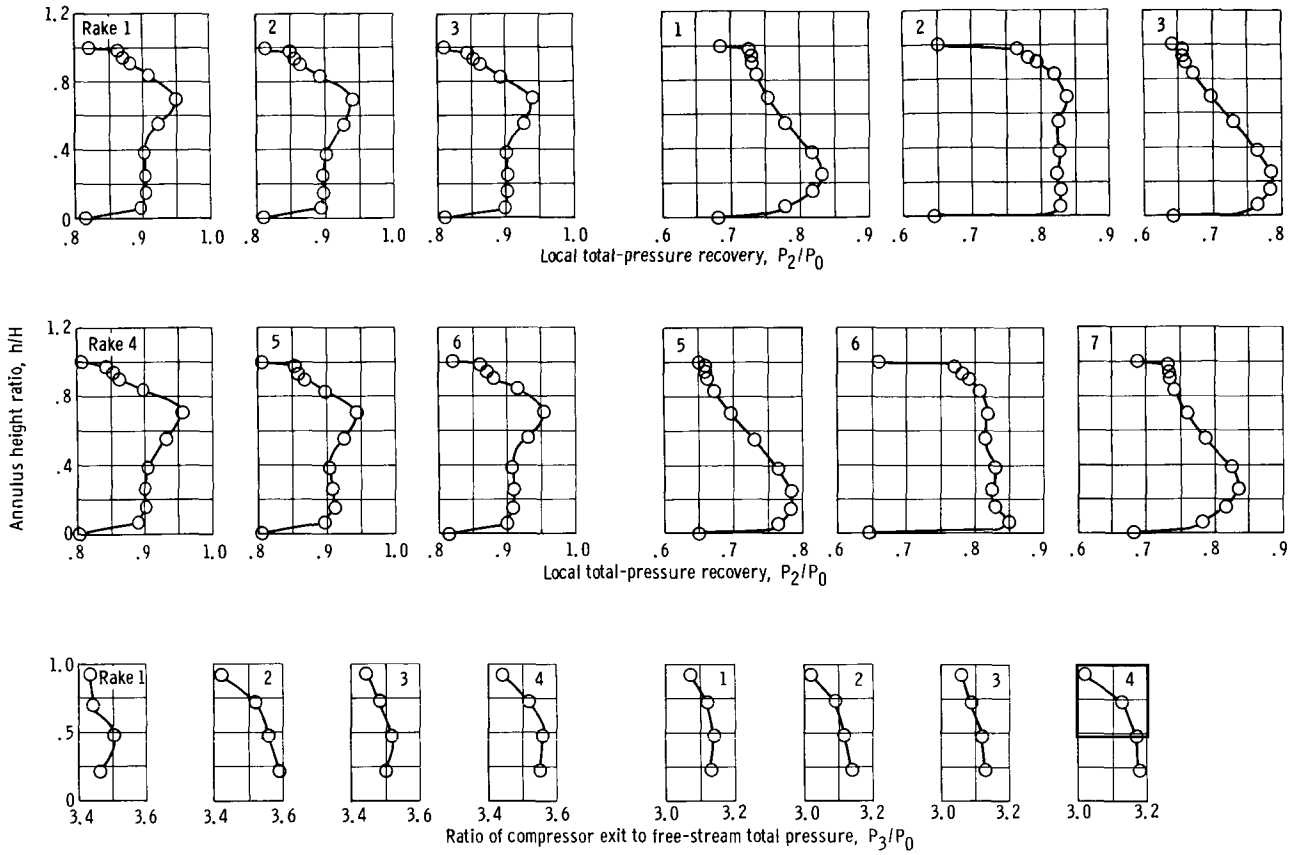

(a) Mach number, 2.5; angle of attack, 0°; total-pressure recovery, $\overline{P}_2/P_0 = 0.907$; compressor face total-pressure distortion, $\Delta P_2/\overline{P}_2 = 0.13$; free-stream total temperature, 294 K.

(b) Mach number, 2.58; angle of attack, 4.3°; total-pressure recovery, $\overline{P}_2/P_0 = 0.764$; compressor face total-pressure distortion, $\Delta P_2/\overline{P}_2 = 0.27$; free-stream total temperature, 339 K.

Figure 11. - Effect of compressor face distortion on compressor exit total-pressure profiles. Compressor exit total-pressure distortion, $\Delta P_3/\overline{P}_3 = 0.05$; corrected engine speed, $N/N^*\sqrt{\theta} = 0.86$.

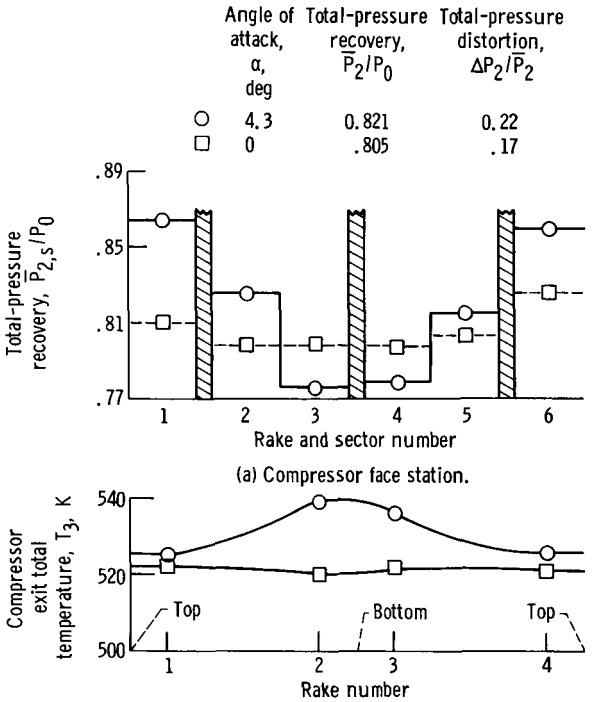

Figure 12. - Effect of compressor face circumferential total-pressure distortion on compressor discharge temperature at Mach 2.58, corrected engine speed, $N/N^*\sqrt{\theta}$ = 0.86, and free-stream total temperature, 339 K.

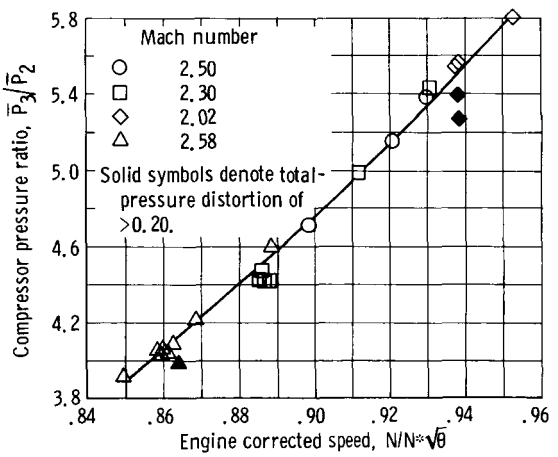

Figure 13. - Effect of high compressor face total-pressure distortion on compressor pressure ratio at ambient temperature, 0° angle of attack, and engine operating with nozzle on cruise flat.

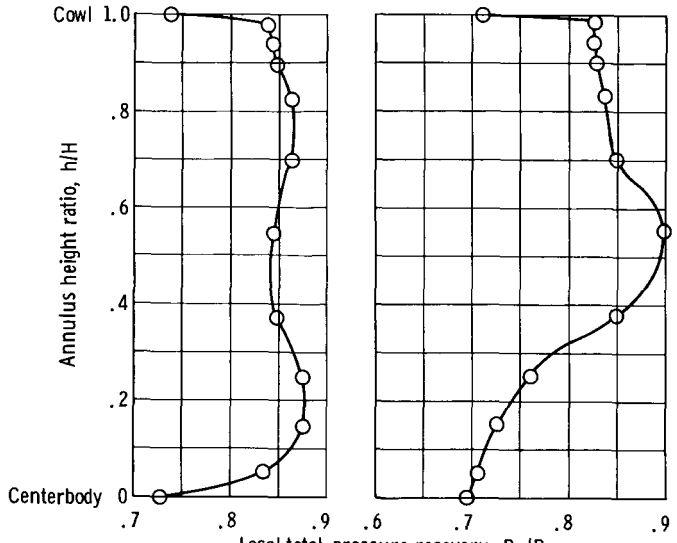

(a) Total-pressure recovery, $\overline{P}_2/P_0 = 0.859$; total-pressure distortion, $\Delta P_2/\overline{P}_2 = 0.09$; compressor pressure ratio, $\overline{P}_3/\overline{P}_2 = 5.54$.

(b) Total-pressure recovery, $\overline{P}_2/P_0 = 0.843$; total-pressure distortion, $\Delta P_2/\overline{P}_2 = 0.26$; compressor pressure ratio, $\overline{P}_3/\overline{P}_2 = 5.28$.

Figure 14. - Comparison of compressor face total-pressure profiles at high and low distortions. Free-stream Mach number, 2.02; angle of attack, 0°; corrected engine speed, $N/N^*\sqrt{\theta} = 0.94$; free-stream total temperature, 294 K.

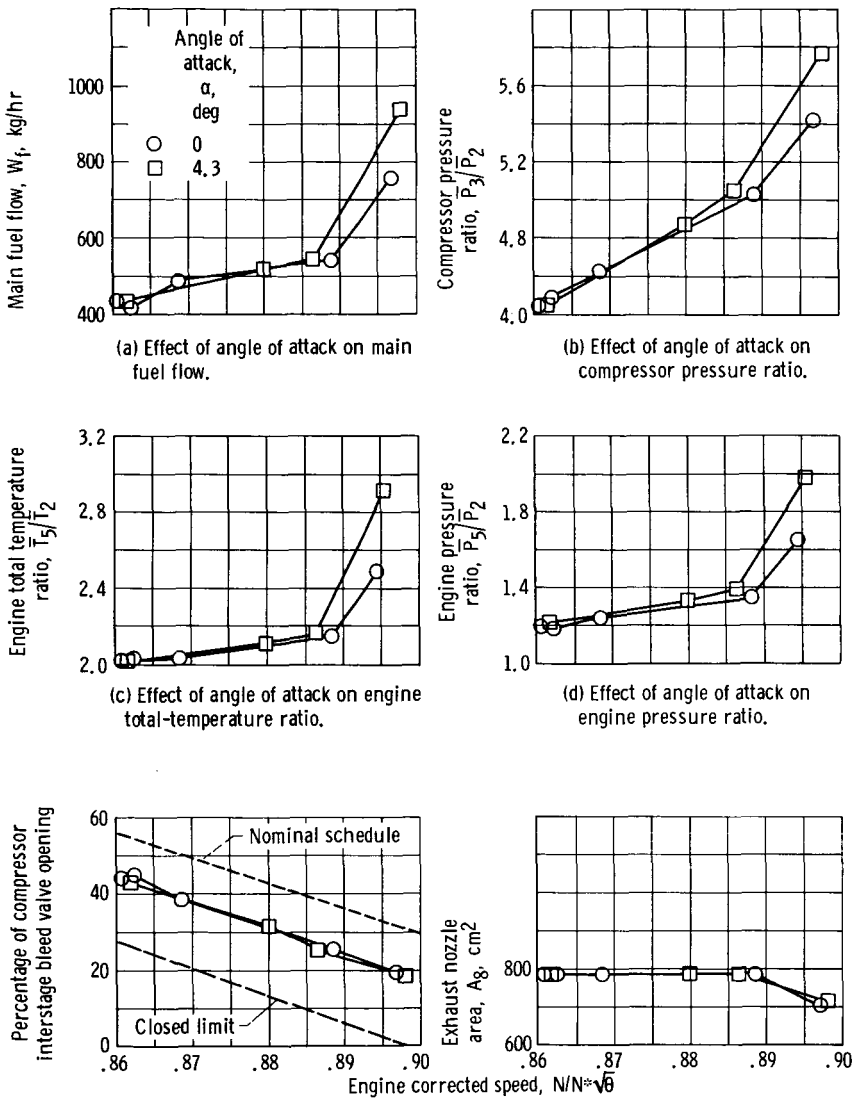

Figure 15. - Effect of angle of attack on engine performance at free-stream Mach number of 2.58 and free-stream total temperature of 339 K.

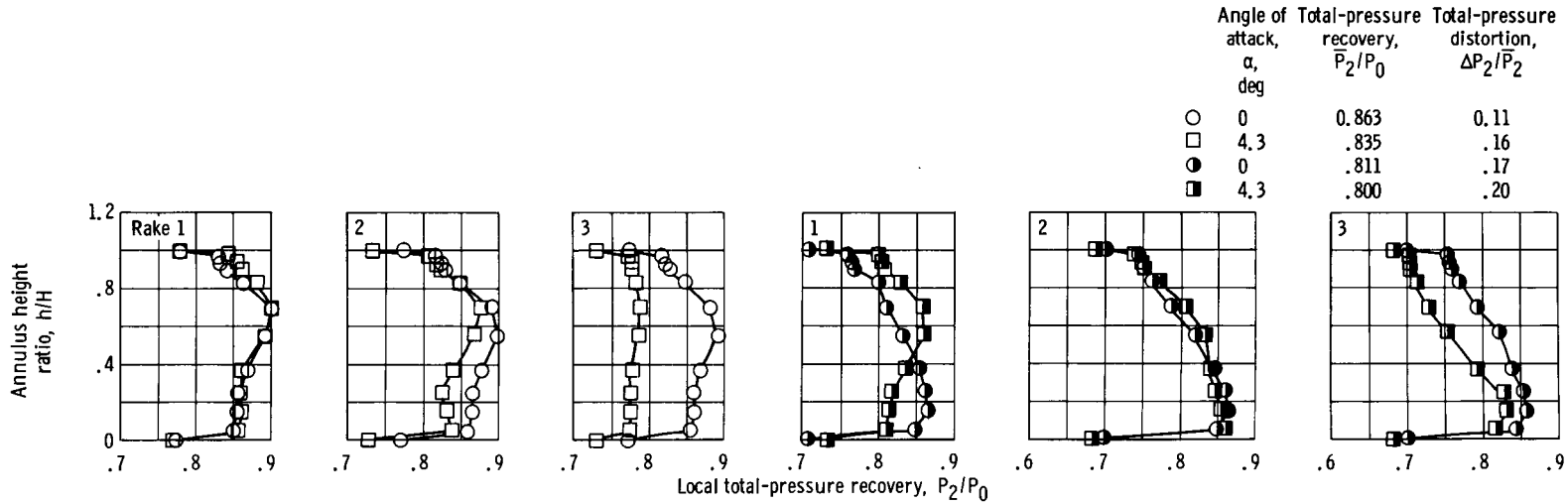

(a) Compressor face total-pressure profiles; engine corrected speed, $N/N^*\sqrt{\theta} = 0.86$.

(b) Compressor face total-pressure profiles; engine corrected speed, $N/N^*\sqrt{\theta} = 0.90$.

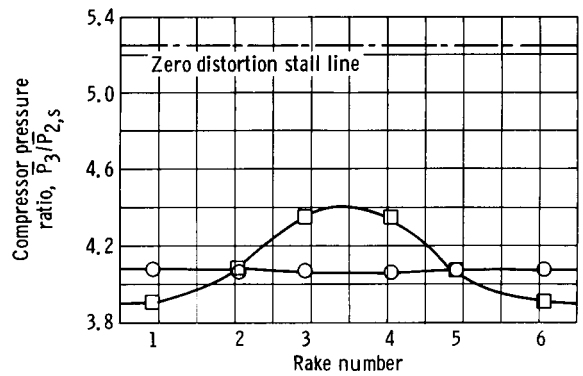

(c) Compressor pressure ratio; corrected engine speed, $N/N^*\sqrt{\theta} = 0.86$.

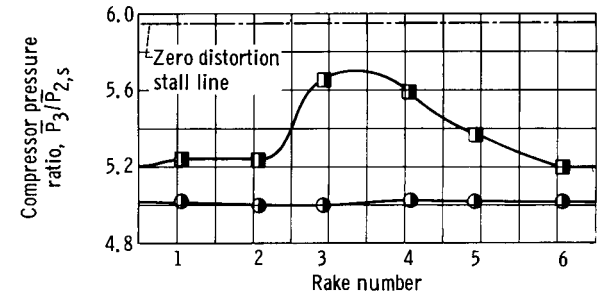

(d) Compressor pressure ratio; corrected engine speed, $N/N^*\sqrt{\theta} = 0.90$.

Figure 16. - Effect of angle of attack on compressor performance at free-stream Mach number of 2.58 and free-stream total temperature of 339 K.